RESEARCH ARTICLE

Translational Physiology

Assessing the degree of hepatic ischemia-reperfusion injury using physiologically based pharmacokinetic modeling of sodium fluorescein disposition in ex vivo machine-perfused livers

Christopher E. Monti,^{1,2}* Seung-Keun Hong,³* Daid H. Audi,^{1,4} Whayoung Lee,⁵ Amit Joshi,¹ Scott S. Terhune,² Doohyun Kim,³* and Ranjan K. Dash^{1,4,6}*

¹Department of Biomedical Engineering, Medical College of Wisconsin, Milwaukee, Wisconsin, United States; ²Department of Microbiology and Immunology, Medical College of Wisconsin, Milwaukee, Wisconsin, United States; ³Division of Transplant Surgery, Department of Surgery, Medical College of Wisconsin, Milwaukee, Wisconsin, United States; ⁴Department of Biomedical Engineering, Marquette University, Milwaukee, Wisconsin, United States; ⁵Department of Pathology, Medical College of Wisconsin, Milwaukee, Wisconsin, United States; and ⁶Department of Physiology, Medical College of Wisconsin, Milwaukee, Wisconsin, United States

Abstract

Ischemia-reperfusion injury (IRI) is an intrinsic risk associated with liver transplantation. Ex vivo hepatic machine perfusion (MP) is an emerging organ preservation technique that can mitigate IRI, especially in livers subjected to prolonged warm ischemia time (WIT). However, a method to quantify the biological response to WIT during MP has not been established. Previous studies used physiologically based pharmacokinetic (PBPK) modeling to demonstrate that a decrease in hepatic transport and biliary excretion of the tracer molecule sodium fluorescein (SF) could correlate with increasing WIT in situ. Furthermore, these studies proposed intracellular sequestration of the hepatocyte canalicular membrane transporter multidrug resistance-associated protein 2 (MRP2) leading to decreased MRP2 activity (maximal transport velocity; V_{max}) as the potential mechanism for decreased biliary SF excretion. We adapted an extant PBPK model to account for ex vivo hepatic MP and fit a six-parameter version of this model to control time-course measurements of SF in MP perfusate and bile. We then identified parameters whose values were likely insensitive to changes in WIT and fixed them to generate a reduced model with only three unknown parameters. Finally, we fit the reduced model to each individual biological replicate SF time course with differing WIT, found the mean estimated value for each parameter, and compared them using a one-way ANOVA. We demonstrated that there was a significant decrease in the estimated value of V_{max} for MRP2 at the 30-min WIT. These studies provide the foundation for future studies investigating realtime assessment of liver viability during ex vivo MP.

NEW & NOTEWORTHY We developed a computational model of sodium fluorescein (SF) biliary excretion in ex vivo machine perfusion and used this model to assess changes in model parameters associated with the activity of MRP2, a hepatocyte membrane transporter, in response to increasing warm ischemia time. We found a significant decrease in the parameter value describing MRP2 activity, consistent with a role of decreased MRP2 function in ischemia-reperfusion injury leading to decreased secretion of SF into bile.

ischemia-reperfusion injury; liver transplantation; machine perfusion; physiologically based pharmacokinetic modeling; sodium fluorescein excretion

INTRODUCTION

Liver transplantation (LT) is considered to be the only definitive treatment for end-stage liver diseases (1). Because of the scarcity of donors and the rising incidence of liver disease (e.g., hepatocellular carcinoma), there is a pressing requirement for

methodologies that not only increase the pool of transplantable organs but also facilitate the assessment of liver viability before LT (2-7). To expand the donor organ pool, there has been an increased adoption of "marginal" organs, characterized by an extended warm ischemia time (WIT), with the aid of machine perfusion (MP) technology (8–10). WIT is defined as the period

*C. E. Monti and S.-K. Hong contributed equally to this work. J. Kim and R. K. Dash contributed equally to this work. Correspondence: R. K. Dash (rdash@mcw.edu); J. Kim (jokim@mcw.edu). Submitted 13 February 2024 / Revised 23 May 2024 / Accepted 17 June 2024



from the cessation of blood flow to the point of perfusion with a cold preservation solution, which critically amplifies the extent of ischemia-reperfusion injury (IRI) (11, 12). Recently, normothermic MP has been associated with better early liver function compared with the traditional static cold storage methods (13). Thus, normothermic, ex vivo MP may represent a strategy for reducing IRI, which ultimately may increase the number of viable organs available for use in LT. Given the relative novelty of this technique, however, there is an eminent need for increased understanding of the physiological changes that occur during hepatic IRI and ex vivo MP.

Bile production has been identified as a tool to assess liver viability for transplantation (14). Furthermore, recent studies have shown that decreased hepatic transport and biliary excretion of the Food and Drug Administration (FDA)approved tracer molecule sodium fluorescein (SF) is associated with increased WIT and hepatic IRI in rats (10, 15). Specifically, SF and its metabolite SF glucuronate (SFG) are transported into the hepatocyte via the organic anionictransporting polypeptide 1B2 (OATP1B2) transporter (16-18). Both SF and SFG are thought to be transported out of the hepatocyte into the sinusoid via the multidrug resistance-associated protein 3 (MRP3) transporter due to structural similarity to other molecules conjugated with fluorescein (17, 19–21). Finally, SF and SFG are thought to be excreted into the bile via the hepatocyte canalicular membrane transporter MRP2 (10, 15, 17). It is thought that, in the presence of hepatic IRI, MRP2 is sequestered inside the hepatocytes, away from the canalicular membrane, decreasing the overall capacity of the hepatocytes to transport SF (and other metabolites) into the bile in a dose-dependent manner (10, 15, 22). Although this has been studied previously in situ, there are currently no studies examining biliary SF excretion kinetics in ex vivo MP livers (10, 15). In addition, datadriven physiologically based pharmacokinetic (PBPK) modeling provides a mechanistic and quantitative approach to connect variations in hepatocyte transport and biliary excretion of SF due to hepatic IRI with variations in physiological parameters representative of the dominant processes defining liver viability through the process of model parameterization.

The primary goal of this study was to 1) develop and parameterize a data-driven PBPK model describing perfusate and biliary SF excretion kinetics during ex vivo MP of livers, 2) use the ex vivo MP liver PBPK model to describe SF kinetic data measured in-house with varying levels of WIT and hepatic IRI, and 3) correlate changes in the model parameter values with increasing WIT and hepatic IRI. We hypothesized that increasing WIT and hepatic IRI will correlate with a decrease in the model parameter value associated with MRP2-mediated SF transport into the bile. We tested this hypothesis by fitting our model to the ex vivo MP SF kinetic data from perfusate and bile with varying levels of WIT. Overall, these studies aim to develop a correlation between WIT and MRP2 activity using quantitative analysis of SF excretion obtained from ex vivo MP rat livers. These studies aim to serve as a foundation for future quantitative research investigating real-time assessment of liver viability during ex vivo MP, which we hope will eventually be able to be used as a clinical benchmark to help inform liver viability during transplant.

MATERIALS AND METHODS

SF Excretion Measurements of Ex Vivo Machine-Perfused Livers with Varying Levels of IRI

To quantify the effects of IRI on hepatocyte bile production, sodium fluorescein (SF) excretion data for ex vivo rat livers undergoing machine perfusion (MP) were obtained using the experimental protocol described in Fig. 1A, which was adapted from Ref. 4. All animals were housed in an animal facility accredited by the Association for Assessment and Accreditation of Laboratory Animal Care. Animals had ad libitum access to Purina LabDiet 5001 and reverse osmosis water. All animals received humane care in accordance with the National Institutes of Health's Guide for Care and Use of Laboratory Animals. The Institutional Animal Care and Use Committee at the Medical College of Wisconsin approved all experiments (application no. 00004857). Briefly, livers from male, anesthetized (1%-3% isoflurane inhalation anesthesia with 1 L/min O₂), Sprague-Dawley rats (Charles River Laboratories) were subjected to 0 (control), 10, 20, or 30 min of warm ischemia time (WIT) (henceforth I10, I20, and I30, respectively) by ligation of the hepatic artery and portal vein using the protocol described. After the designated WIT, the infrahepatic IVC was ligated, the portal vein was cannulated with a 16-gauge catheter, and the bile duct was cannulated with polyethylene tubing (PE10; Braintree Scientific). The chest cavity was opened, and the suprahepatic IVC was cannulated with PE10 tubing. Livers were flushed with 50 mL of lactated Ringer's solution with 50 units of heparin (SAGENT Pharmaceuticals), removed from the body cavity, and then subjected to cold ischemia time (CIT) using cold lactated Ringer's solution while the MP system was prepared. To ensure consistent cold ischemic injury across all samples, in addition to varying WIT, we incorporated 3 h of CIT for all livers. This also provided adequate and uniform preparation time for ex vivo machine perfusion setup in this experiment.

Next, livers were perfused for 1 h using the custom ex vivo MP system described in Ref. 4. In brief, the normothermic machine perfusion system was primed with 100 mL of perfusate [Dulbecco's modified Eagle's medium = 72.3 mL, human 4% albumin = 3.2 mL, human insulin aspart (100 IU/mL) = 2 mL, penicillin-streptomycin (10,000 U/mL) = 1 mL, L-glutamine (200 mM) = 1 mL, porcine packed red blood cell = 20 mL, heparin (1,000 U/mL) = 0.5 mL, and taurocholic acid sodium salt = 25 mg] in a glass reservoir, which was placed on a magnetic stirrer maintaining a temperature of $\sim 38^{\circ}$ C. The system was connected to a peristaltic pump and the oxygenator. The portal vein was connected to the inflow of the system, and the suprahepatic IVC was connected to the outflow. The initial flow rate was set at 5 mL/min and was increased by 5 mL/min every 5 min up to a maximum of 30 mL/min or 12 mmHg of portal venous pressure. Subsequently, 0.4 mg/kg (total rat weight) of SF (Sigma-Aldrich) was injected into the reservoir perfusate at the end of the 1-h period. Finally, SF fluorescence measurements in the perfusate and bile were taken at indicated time points using a CLARIOstar (BMG Labtech, Ortenberg, Germany) microplate reader set at excitation wavelength of 478 nm and emission wavelength of 505-552 nm using a gain of 1,000 for perfusate and 500 for bile (15). Fluorescence measurements for five (IRI) or six (control)

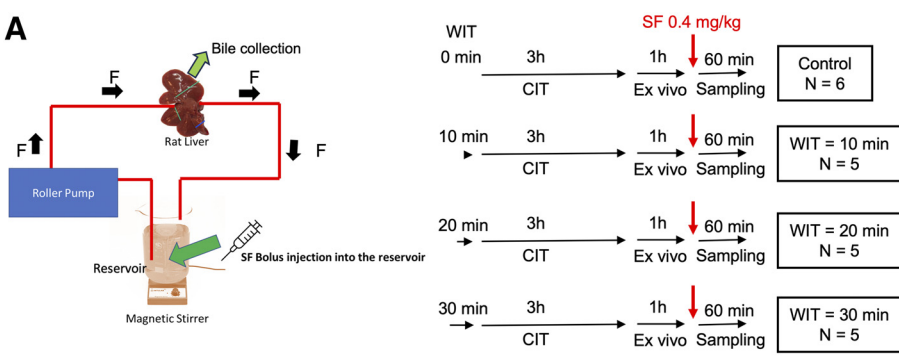
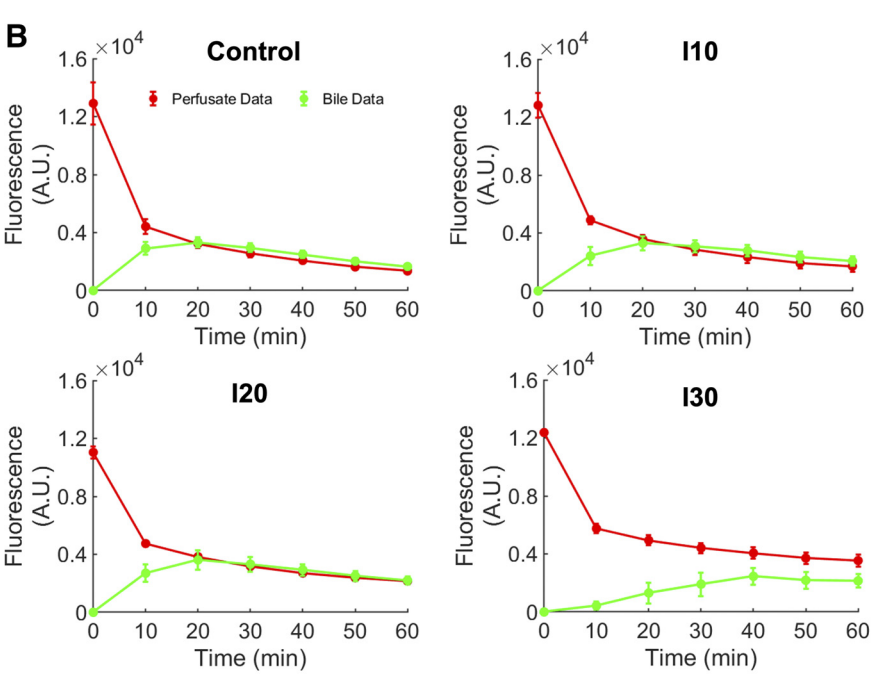


Figure 1. Experimental ex vivo liver machine perfusion (MP) data obtained by The Dr. Joohyun Kim Laboratory (Froedtert Hospital Division of Transplant Surgery). A: schematic of the ex vivo liver MP experimental setup (left) and experimental timeline (right). B: sodium fluorescein (SF) fluorescence measurements in perfusate and bile over 60 min with varying levels of warm ischemia time (WIT). Data are means \pm SE (n=5 or 6 biological replicates).



biological replicates from MP perfusate and bile for each IRI duration are presented in Fig. 1B. Time-course fluorescence measurements for individual rats can be found in Supplemental Fig. S1.

Calibration of Fluorescent Measurements and Conversion to Units of Concentration

To convert between units of fluorescence and concentration, calibration curves were developed relating the two quantities in both perfusate and bile background matrices. These calibration curves are presented in Fig. 2A. Known quantities of SF (x-axis) were spiked into MP perfusate, and SF fluorescence was measured (*y*-axis). Linear regression was performed to generate a relationship between SF fluorescence and concentration in MP perfusate. The bile calibration curve was adapted from Ref. 10. Individual fluorescence measurements from Fig. 1B were then converted to units of concentration by first subtracting background values (i.e., fluorescence at t = 0 min) and then converting to concentration units via the calibration curve (Fig. 2B). The calibrated time-course concentration measurements for individual rats can be found in Supplemental Fig. S2. Of note, experimental parameters (e.g., perfusate flow rates, bile volumes) were

recorded simultaneously with fluorescence measurements. To maximize the number of complete datasets available for modeling, any missing experimental variables for specific time points were filled in with the mean of the prior and subsequent time points containing values for that variable for a particular replicate.

Development of Ex Vivo Liver MP Computational Model

Figure 1A (left) shows a blueprint of the liver MP system involving hepatic transport and biliary excretion. This information was then translated into a schematic of SF biliary excretion during ex vivo liver MP (Fig. 3). This schematic was the foundation for the generation of the ordinary differential equations (ODEs) for the physiologically based pharmacokinetic (PBPK) model used in subsequent analyses. In this schematic, SF is injected into the perfusate-containing reservoir of the MP system over a short duration. The total volume of the reservoir $(V_{R,tot})$ is 100 mL. Given the brevity of the injection process, it was appropriate to set the initial concentration of SF [rat weight \times 0.4 (mg/kg)/ V_{R1}] in the injection reservoir (reservoir 1) to be the initial condition for this region; V_{R1} (reservoir 1 volume) is estimated from the measured initial concentration of SF in reservoir 1 for each

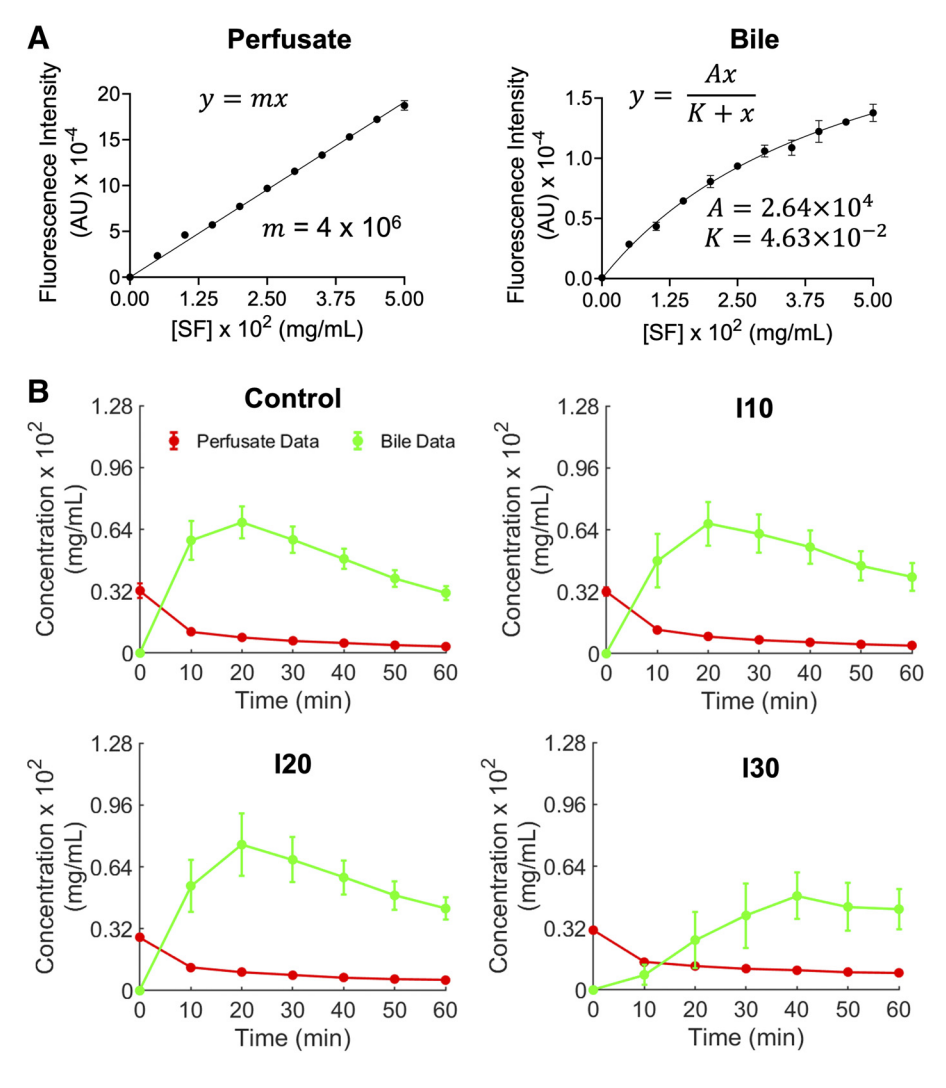


Figure 2. Conversion of fluorescence measurements to concentration measurements for use in computational models. A, left: calibration curve showing a linear relationship between SF fluorescence and concentration in ex vivo liver machine perfusion perfusate obtained by The Dr. Joohyun Kim Laboratory (Froedtert Hospital Division of Transplant Surgery). Right: nonlinear calibration curve relating SF concentration in bile to SF fluorescence obtained previously (10). B: conversion of fluorescence data in Fig. 1B to concentration units. Data are means \pm $S\bar{E}$ (n=5 or 6). SF, sodium fluorescein.

experiment. In addition, we assumed that perfusate sampling occurred from reservoir 1. Although a stir bar was present, allowing for mixing, we found through iterative model design that it was necessary to account for incomplete mixing by adding a mixing region (reservoir 2), which communicates with the rest of the MP system and has volume $V_{\rm R,2} = 100 - V_{\rm R,1}$ mL. Thus, SF is injected into reservoir 1 and can then diffuse into reservoir 2 (characterized by mixing constant K_{mix}). For simplicity, we defined K_{mix} to be a constant fraction (α) of the flow F. Once in reservoir 2, the SFcontaining perfusate is pumped (characterized by perfusate flow rate F) through a short amount of tubing into the ex vivo liver. The minimal tubing volume (~1 mL) and relatively high flow rate (~25 mL/min) compared with sampling rate allowed for the use of computationally simple ODEs rather than partial differential equations to account for the dispersion (convection and diffusion) of SF through the tubing (23) (Transit time = 1 mL/25 mL/min = 0.04 min transittime \ll 10 min sampling time).

The subsequent portions of this PBPK model are adapted from Ref. 10. Briefly, SF-containing perfusate enters the hepatic sinusoids where SF and its metabolite SF monoglucuronide (SFG) can be transported into or out of the hepatocytes via OATP1B2 and MRP3 transporters, respectively, on the

hepatocyte basolateral membrane. The remaining SF and SFG in the perfusate are returned to reservoir 2 via pumping (F). Once inside the hepatocyte, SF can be converted to SFG via a glucuronidation reaction (SF metabolism) or SF and SFG can be transported into the bile via the MRP2 transporter on the hepatocyte canalicular membrane. Once inside the bile, SF is cleared via an experimentally cannulated bile duct (characterized by bile flow rate $F_{\rm B}$) (Fig. 3).

Using this schematic, model ODEs were developed using mass balance accounting for mixing, convective transport, and the action of hepatocyte glucuronide enzyme and membrane proteins (OATP1B2/MRP3 and MRP2). For mixing and convective processes, concentration gradients were considered to account for the thermodynamic driving force. For unidirectional enzymatic and transport processes, appropriate Michaelis-Menten equations were implemented (10, 24):

$$JS = \frac{dC_P}{dt} = \frac{V_{max}C_S}{K_m + C_S}. \tag{1}$$

This equation provides the unidirectional flux for a specific substrate (J_S) through an enzyme or transport process, where C_S and C_P are substrate and product concentrations, respectively, for an enzymatic process. Using simple Michaelis-

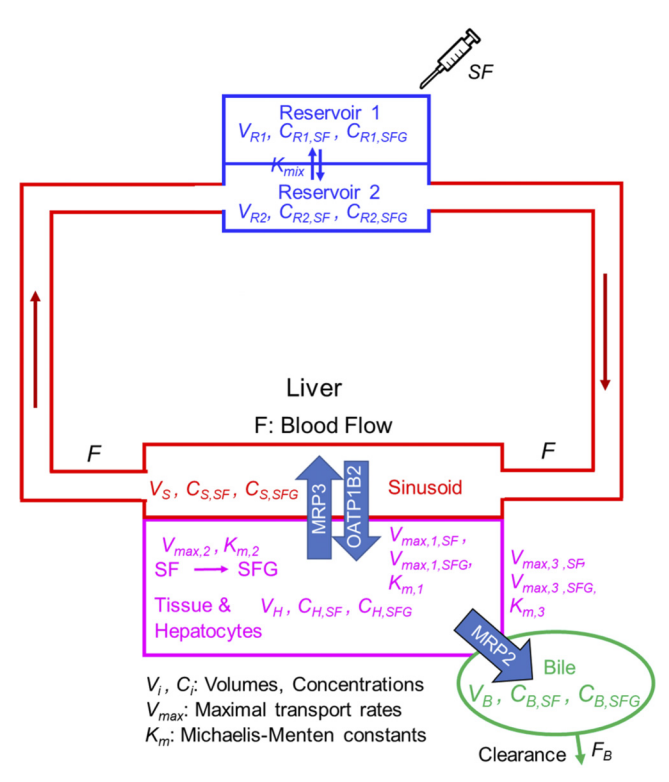


Figure 3. Model schematic adapted from Monti et al. (10) with permission to account for ex vivo liver machine perfusion. SF is injected into the perfusate reservoir (reservoir 1), which is then mixed into the remainder of the reservoir (reservoir 2) that connects to the ex vivo rat liver. SF-containing perfusate enters the liver sinusoids (sinusoid), where SF and its conjugate SF monoglucuronide (SFG) are transported into and out of the hepatocytes via the combined action of the OATP1B2/MRP3 transporters. Once inside the hepatocytes, SF is converted to SFG via a glucuronidation reaction, and both SF and SFG are transported into the bile via the MRP2 transporter. This model has a maximum of six parameters for which physiological values (particularly during IRI) are unknown: $V_{\text{max,1,SF}}$, $V_{\text{max,1}}$ sFG, $V_{\text{max,3,SF}}$, $V_{\text{max,3,SFG}}$, and K_{mix} . MRP3, multidrug resistance-associated protein 3; OATP1B2, organic anionic-transporting polypeptide 1B2; SF, sodium fluorescein.

Menten kinetics, the glucuronidation reaction of SF to SFG can be expressed as:

$$J_2 = \frac{V_{\text{max,2}} C_{\text{H,SF}}}{K_{\text{m,2}} + C_{\text{H,SF}}}.$$
 (2)

We then sought to apply the concept of Michaelis-Menten kinetics to membrane transport facilitated by transport proteins. We hypothesized that, given the structural similarity between SF and SFG, and the fact that SF and SFG use the same transporters, the two compounds would likely compete for binding spots on transport proteins as has been shown previously (25, 26). However, the maximal transport velocity ($V_{\rm max}$) would likely differ between the molecules due to different catalytic activities for SF and SFG (27). Specifically, we hypothesize that $V_{
m max,SFG}$ would likely be greater than $V_{
m max,SF}$ due to increased water solubility of SFG, leading to a higher catalytic activity and faster overall transport across the hepatocyte membrane via a transporter (28, 29). To account for this hypothesis, we defined $V_{\rm max,1,SFG}$ and $V_{\rm max,3,SFG}$ to be directly proportional to $V_{\text{max},1,\text{SF}}$ and $V_{\text{max},3,\text{SF}}$ with

proportionality constants >1 (β_1 and β_2 , respectively). Thus, *Eq. 1* for unidirectional transport of SF becomes:

$$J_{\rm SF} = \frac{V_{\rm max,SF} \frac{C_{\rm SF}}{K_{\rm m,SF}}}{1 + \frac{C_{\rm SF}}{K_{\rm m,SF}} + \frac{C_{\rm SFG}}{K_{\rm m,SFG}}} \tag{3}$$

and a similar equation can be written for SFG incorporating the appropriate β term (30). As in Ref. 10, we hypothesized that the Michaelis-Menten constants ($K_{m,SF}$ and $K_{m,SFG}$) would likely remain similar between the SF and SFG. Thus, Eq. 3 reduces to:

$$J_{\rm SF} = \frac{V_{\rm max,SF}C_{\rm SF}}{K_{\rm m} + C_{\rm SF} + C_{\rm SFG}} \tag{4}$$

and a similar equation can be written for SFG. This formulation is appropriate for the unidirectional transport of SF and SFG via the irreversible MRP2 transporter on the hepatic canalicular membrane. Thus, the flux equation for the MRP2 transporter for SF or SFG from the hepatocyte into the bile can be written as:

$$J_{X,3} = \frac{V_{\text{max,3,X}}C_{\text{H,X}}}{K_{m,3} + C_{\text{H,SF}} + C_{\text{H,SFG}}},$$
 (5)

where C_H represents concentration in the hepatocyte and X is either SF or SFG.

For the bidirectional transport of SF and SFG via the reversible OATP1B2/MRP3 transporter on the hepatic basolateral membrane, we assumed these transporters are coupled, thereby functioning as a single transporter as in Ref. 10. Incorporating this assumption, the bidirectional transport flux equation for OATP1B2/MRP3 can be appropriately derived:

$$J_{X,1} = \frac{V_{\text{max,1,X}}(C_{S,X} - C_{H,X})}{K_{m,1} + C_{S,SF} + C_{H,SF} + C_{S,SFG} + C_{H,SFG}},$$
 (6)

where C_S is the concentration in the sinusoid, C_H is the concentration in the hepatocyte, and X is either SF or SFG.

Using these flux terms and mass balance, ODEs describing the model schematized in Fig. 3 can now be developed:

$$V_{R1} \frac{dC_{R1,SF}}{dt} = K_{mix} (C_{R1,SF} - C_{R2,SF})$$
 (7)

$$V_{R1} \frac{dC_{R1,SFG}}{dt} = K_{mix} (C_{R1,SFG} - C_{R2,SFG})$$
 (8)

$$V_{R2} \frac{dC_{R2,SF}}{dt} = K_{mix} (C_{R1,SF} - C_{R2,SF}) - F(C_{R2,SF} - C_{S,SF})$$
 (9)

$$V_{R2} \frac{dC_{R2,SFG}}{dt} = K_{mix} (C_{R1,SFG} - C_{R2,SFG}) - F(C_{R2,SFG} - C_{S,SFG})$$
 (10)

$$V_{S} \frac{dC_{S,SF}}{dt} = F(C_{R2,SF} - C_{S,SF}) - J_{1,SF}$$
 (11)

$$V_{S} \frac{dC_{S,SFG}}{dt} = F(C_{R2,SFG} - C_{S,SFG}) - J_{1,SFG}$$
 (12)

$$V_{H} \frac{dC_{H,SF}}{dt} = J_{1,SF} - J_{2} - J_{3,SF}$$
 (13)

$$V_{\rm H} \frac{dC_{H,\rm SFG}}{dt} = J_{1,\rm SFG} + J_2 - J_{3,\rm SFG}$$
 (14)

$$V_{B} \frac{dC_{B,SF}}{dt} = J_{3,SF} - F_{B}C_{B,SF}$$
 (15)

Table 1. Physiological parameters

Parameter	Description	Value	Units	Reference
Dose	Initial dose of SF injected into reservoir 1	0.40	mg/kg	Experimentally determined
Rat weight	Average rat weight of biological replicates	0.36	kg	Experimentally determined
$V_{R,tot}$	Total volume of perfusate in MP reservoir	100	mL	Experimentally determined
Liver density	Conversion between liver weight and volume	1.00	g/mL	(31)
Vs	Fraction of liver volume accounted for by the sinusoids	0.18	mL	(31)
V_H	Fraction of liver volume accounted for by hepatocytes	0.28	mL	(31)
V_B	Fraction of liver volume accounted for by bile	4.00×10^{-3}	mL	(31–33)
K _{m.1}	Michaelis-Menten constant for SF/SFG influx into hepatocytes	9.30E-03	mg/mL	(18)
K _{m.2}	Michaelis-Menten constant for SF conversion to SFG	0.21	mg/mL	(10)
K _{m,3}	Michaelis-Menten constant for SF/SFG efflux into bile	5.80E-04	mg/mL	(10)

SF, sodium fluorescein; SFG, SF monoglucuronide.

$$V_{\rm B} \frac{dC_{B,\rm SFG}}{dt} = J_{3,\rm SFG} - F_{\rm B}C_{\rm B,SFG}.$$
 (16)

Here, $V_{\boldsymbol{X}}$ is the volume of a region X. Model ODEs were then solved using the MATLAB (MathWorks) ode15s function, with experimentally measured initial concentration of SF in the perfusate in *reservoir 1* and zero initial concentrations for all other variables in all other regions. In this model, there are six parameters for which values are potentially unknown: $V_{\text{max,1,SF}}$, β 1, $V_{\text{max,2}}$, $V_{\text{max,3,SF}}$, β 2, and α (Table 2). Average values for other known physiological parameters can be found in Table 1.

Parameter Estimation and Quality Control

Unknown parameters were estimated using a pseudo-Monte Carlo parameter estimation protocol described in Ref. 34. Briefly, a sum-squared error (SSE) function was used to compare between the model solution and the measured data on SF concentrations in the perfusate in reservoir 1 and in the bile. This SSE function was weighted to approximately equalize the contributions of the bile and perfusate SF datasets to the total SSE (see Fig. 1B)

$$SSE_{perfusate} = \Sigma \left(\frac{Model_{perfusate} - Data_{perfusate}}{max(Data_{perfusate})} \right)^{2}$$
 (17)

$$SSE_{bile} = \Sigma \left(\frac{Model_{bile} - Data_{bile}}{max(Data_{bile})} \right)^{2}$$
 (18)

$$SSE_{tot} = 2 \times SSE_{perfusate} + SSE_{bile}. \tag{19}$$

The MATLAB function fmincon was used to minimize the SSE function with the interior point optimization algorithm using random initial guesses (34, 35). Parameter estimates were randomized from their initial guesses, and estimates were bounded between 1/10 and 10 times their initial values, except for the flow fraction parameter α for K_{mix} , which was bounded between 0.2 and 1. Parameters were estimated 1,000 times to generate distributions for individual parameters. Finally, the parameter set with the most frequently estimated values is presented in Table 2. Insensitive model parameters were fixed (see RESULTS) and subsequent modeling analysis used only one iteration of fitting. Table 3 shows parameters estimated by fitting to average datasets for control and IRI conditions, and parameter sets for fitting to individual replicates can be found in Supplemental Table S1. Nested models (i.e., models formulated from the same schematic but with a smaller number of unknown parameters) can be evaluated using the *F*-statistics:

$$F = \frac{df_B}{SSE_R} \left(\frac{SSE_A - SSE_B}{df_A - df_B} \right), \tag{20}$$

where A is the simpler model with less estimated parameters; B is the more complex model with more estimated parameters; df is the degrees of freedom, which is the difference in the number of data points (14 data points) and the number of estimated parameters (3 or 6 parameters); and SSE is the sum-squared error. The F-statistic can then be used to obtain a P value using the F distribution, which can help determine if the increase in model complexity due to additional parameters is justified by a sufficient decrease in SSE (34, 36).

Error sensitivity plots help to assess the contribution of each parameter to the SSE cost function. The SSE for the final optimal parameter set selected through pseudo-Monte Carlo parameter estimation (p_0) is calculated (SSE₀). Next, each parameter is individually increased or decreased by a small amount (p) and the SSE is recalculated (SSE). The ratios of p/p_0 and SSE/SSE₀ are then plotted as x,y-pairs. This process is repeated until the parameter is changed by 0.5 or 1.5 times its original value. The entire procedure is then repeated for each parameter and plotted.

RESULTS

Effects of WIT on SF Excretion during MP

The time-course data for sodium fluorescein (SF) excretion into bile from perfusate during machine perfusion (MP) with increasing warm ischemia time (WIT) are shown in

Table 2. Six-parameter model estimates

Parameter	Value	Units
F	23.50	mL
F_{B}	0.01	mL/min
$V_{R,1}$	41.60	mL
$V_{R,2}$	58.40	mL
Total rat liver volume	17.78	mL (31)
$V_{max,1,SF}$	1.50	mg/min
$\beta_1 \left(V_{\text{max,1,SF}} / V_{\text{max,1,SFG}} \right)$	3.00	mg/min
$V_{\text{max},2}$	0.23	mg/min
$V_{\text{max,3,SF}}$	2.25×10^{-4}	mg/min
$\beta_2 \left(V_{\text{max,3,SF}} / V_{\text{max,3,SFG}} \right)$	12.50	mg/min
$\alpha (F/K_{mix})$	2.58	Unitless

Table 3. Three-parameter model estimates

Parameter	WIT	Value	Units
Estimated			
$V_{\rm max.2}$	0	0.19	mg/mL
	10	0.14	
	20	0.15	
	30	0.04	
$V_{\rm max,3,SF} \times 10^4$	0	2.01	mg/mL
	10	1.72	
	20	1.58	
	30	0.30	
α (F/K _{mix})	0	2.74	Unitless
	10	2.79	
	20	2.52	
	30	3.55	
Experimentally determined	_	44.00	1
$V_{R,1}$	0 10	41.60 41.91	mL
	20	41.91	
	30	43.41	
$V_{R,2}$	0	58.40	mL
▼ R,2	10	58.09	111L
	20	51.35	
	30	56.59	
F	0	23.50	mL/min
	10	18.40	
	20	18.71	
	30	15.37	
F _B	0	0.01	mL/min
	10	0.01	
	20	0.01	
	30	3.00×10^{-2}	
Fixed			
V _{max,1,SF}	N/A	1.50	mg/min
$V_{\text{max,1,SFG}}/V_{\text{max,1,SF}}$	N/A	3.00	mg/min
$V_{\text{max,3,SF}}/V_{\text{max,3,SFG}}$	N/A	12.50	Unitless
K _{m,1}	N/A	9.30×10^{-3}	mg/mL
K _{m,2}	N/A N/A	0.21	mg/mL
K _{m,3}	N/A N/A	5.80×10^{-4} 3.20	mg/mL mL
V_{S} V_{H}	N/A N/A	3.20 14.58	mL
	N/A N/A	0.07	mL
V _B	IN/A	0.07	IIIL

WIT, warm ischemia time.

Fig. 2B. Raw fluorescence values for SF in perfusate and bile are shown in Fig. 1B. After 10 min, concentrations of SF were larger in bile than in perfusate, indicating that the liver is concentrating SF in the bile over the 60-min sampling period. Perfusate kinetics show a two-phase decay with an initial fast phase between \sim 0 and 20 min postinjection followed by a slower phase between 20 and 60 min. Bile kinetics show an initial peak around 20 min followed again by a gentle decay. In general, the kinetic profiles for each condition were similar; however, qualitatively, the largest shift in kinetic profile was elicited with 30 min WIT, over the 60-min sampling period. Finally, bile kinetics for 0 min WIT show similar kinetic trends to previous investigations using in situ livers, providing corroboration for our methodology (15).

Fitting and Analysis of Ex Vivo Liver MP Model to **Control Dataset**

The solution of the model described in the previous section and schematized in Fig. 3 was fit to the mean of each timepoint SF concentrations in the reservoir 1 perfusate and in the bile for the control dataset (Fig. 2B, top left) using six unknown parameters and a pseudo-Monte Carlo parameter

estimation protocol described previously (34). Histograms showing the frequency of estimation for the value of each parameter are shown in Fig. 4A. Histograms showing a small range of estimated values for a particular parameter indicate that this parameter is likely estimable within a relatively narrow range. Conversely, a large range of estimated values for a particular parameter indicates that the model is relatively insensitive to a change in the value of that parameter over a wide range, that it is not estimable, and that the parameter should likely be fixed in subsequent analysis given the data available for fitting. Histograms for $V_{\text{max},2}$ and $V_{\text{max},3,\text{SF}}$ show a large peak at their most frequently estimated values as well as an overall small range of estimated values. In contrast, $V_{\text{max,1.SF}}$ shows a more flat distribution with a much larger range (i.e., the most frequently estimated value is 1.5 mg/ min and the range is between 0 and 3 mg/min). In addition, β_1 and β_2 show a large range of estimated values, and β_1 in particular shows a relatively flat distribution. Finally, α does show a highly frequently estimated value; however, the range of values is somewhat intermediate. This is expected as α is related to experimental factors that are likely only partially accounted for by the model. Figure 4B shows the results of fitting the six-parameter model to the perfusate and bile datasets, which readily describe the data. Table 2 shows the estimated values of parameters from this fitting. Specifically, $V_{\text{max},1}$ for both SF and SF monoglucuronide (SFG) and $V_{\text{max},2}$ were approximately three orders of magnitude larger than $V_{\text{max,3,SF}}$ and two orders of magnitude larger than $V_{\text{max,3,SFG}}$. Moreover, the ratio of $V_{\text{max,1,SFG}}$ to $V_{\text{max,1,SF}}$ (β_1) was estimated to be 3, whereas the ratio of $V_{\text{max},3,\text{SFG}}$ to $V_{\text{max,3,SF}}$ (β_2) was estimated to be 12.5, consistent with what we hypothesized. Figure 4C shows how changing each model parameter contributes to a change in the SSE function. It is readily surmised that the two parameters with the largest contribution to a change in SSE are $V_{\text{max},2}$ and $V_{\text{max},3,\text{SF}}$. These data corroborate the findings from the histograms in Fig. 4A, which indicate that $V_{\text{max,1,SF}}$, β_1 , and β_2 are insensitive parameters and can be fixed in subsequent modeling analysis.

We then simulated SF and SFG kinetics over an extended timescale (2 h) and predicted SF and SFG concentrations in all model regions (Fig. 4D). SF concentrations are predicted to peak in reservoir 2, sinusoids, and hepatocytes around 10 min and to peak in the bile around 20 min. Appreciable levels of SF are predicted to be found in the bile beyond 120 min, whereas SF concentration is predicted to approach undetectable levels around 80 min in all other regions. The peak concentration of SFG in the bile is predicted to be around one order of magnitude larger than the peak SF concentration. This makes sense given that SF is consumed through glucuronidation conversion to SFG and due to the fact that both $V_{\text{max,1,SFG}}$ and $V_{\text{max,3,SFG}}$ are estimated to be larger than their respective SF counterparts (Table 2), consistent with our hypothesis. The concentration of SFG in all other regions is predicted to be at least two orders of magnitude lower than the SFG concentration in the bile. This is again due to the large estimated values for $V_{\text{max,1,SFG}}$ and $V_{\text{max},3,\text{SFG}}$ "pulling" SFG through hepatocytes into the bile. We examined the biliary flux of SF and SFG in Fig. 4E (17). Given that deposition of SF and SFG into the bile is achieved through the $J_{3,SF}$ and $J_{3,SFG}$ terms in Eqs. 13–16, the biliary

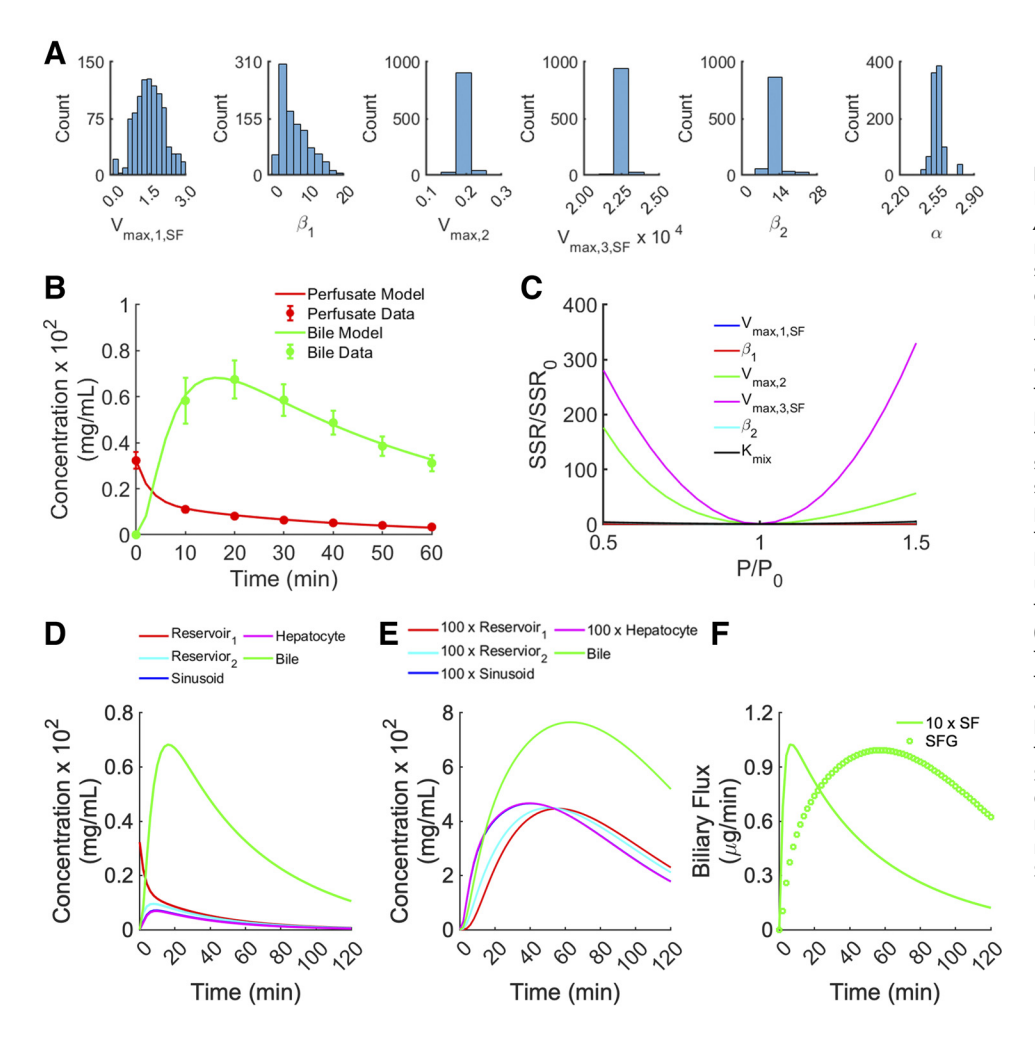


Figure 4. Fitting of the six-parameter PBPK ODE model to the control dataset. A: histograms showing frequency of estimated values for each parameter in the six-parameter ODE model fit to the control dataset using a pseudo-Monte Carlo parameter estimation approach (34) with 1,000 iterations. B: fits of the perfusate and bile SF models (schematized in Fig. 3) to the control dataset (Fig. 2B) using pseudo-Monte Carlo parameter estimates. The estimated parameter values are presented in Table 2. C: model sensitivity plot showing the contribution of varying each parameter to the sum squared error (SSE) function. Model parameters were varied between 0.5 and 1.5 times their original values (po) and the SSE was calculated and then plotted relative to its original value (SSE₀). Results from this analysis indicate that $V_{\text{max,3.SF}}$ and $V_{\text{max,2}}$ are large contributors to the sensitivity of the SSE function. D and E: Simulations of all model state variables for SF (D) and SFG (E) over an extended time course. F: simulations of biliary flux of SF and SFG over an extended time course. ODE, ordinary differential equation; PBPK model, physiologically based pharmacokinetic model; SF, sodium fluorescein; SFG, SF monoglucuronide.

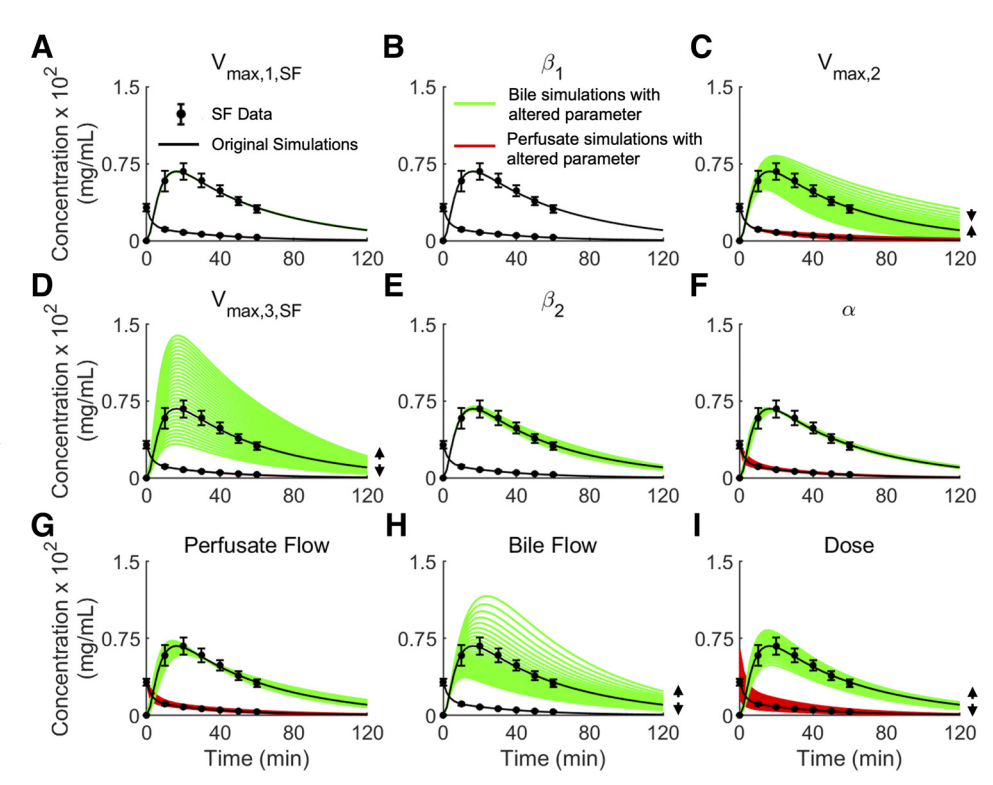
flux plots in Fig. 4B show the magnitudes of these terms over time. Although the relative magnitude of biliary flux of SF is smaller than that of SFG, the shape of the SFG curve and the time scale of SFG excretion were protracted relative to those for SF.

Simulations Showing the Effects of Changing Model **Parameters and Model Reduction**

Previous studies identified a decrease in MRP2 activity as a putative marker for in situ hepatic ischemia-reperfusion injury (IRI) (10, 15). These studies hypothesized that a decrease in MRP2 activity ($V_{\text{max,3,SF}}$) led to a proportional decrease in biliary SF and that this could potentially be correlated with WIT and, by extension, degree of hepatic IRI (10, 15). To test this hypothesis for ex vivo MP livers, we simulated perfusate and biliary SF kinetics with changing model parameters. We varied individual parameters between 0.5 and 1.5 times their original values and simulated perfusate and bile SF kinetics with all other parameters remaining constant (Fig. 5). In addition, we also simulated changes in perfusate flow rate (Fig. 5G), bile flow rate (Fig. 5H), and dose (Fig. 5I) to analyze changes in experimentally determined factors. Figure 5, C and D, clearly demonstrates that $V_{\text{max},2}$ and $V_{\text{max}.3.SF}$ have the largest response to a change in the

model parameter value, consistent with model SSE sensitivity results in Fig. 4C. Furthermore, the directional arrows for $V_{\text{max,2}}$ (Fig. 5C) indicate that its response in the bile is inversely related to the direction of the parameter change (i.e., an increase in $V_{\text{max,2}}$ leads to a decrease in the biliary SF and vice versa). Conversely, biliary SF shows a high degree of sensitivity toward changes in $V_{\text{max,3,SF}}$, however, with correct directionality (Fig. 5D). Previous results show similar trends and corroborate our modeling studies (10). To provide further model validation, we examined the effects of changing experimental model parameters on model predictions. We hypothesized that changes in experimental model parameters such as perfusate flow rate, bile flow rate, and SF dose would lead to proportional changes in the biliary SF kinetics (Fig. 5, G-I). Overall, biliary SF simulations with varied experimental conditions supported this hypothesis and corroborated our model predictions; however, changes in perfusate flow rate showed a blunted response (Fig. 5G). This is due to the fact that, at the range of flow rates analyzed, the system is flow-limited and larger changes were necessary for a less blunted response. These changes may not be practically relevant, however, as a certain vascular pressure is required to maintain the viability of the liver during MP (37).

Figure 5. A-I: model simulations showing the effect of changing single model parameters between 0.5 and 1.5 times their original values on the measured state variables. Note that the most noticeable change occurs when $V_{\rm max,2}$, $V_{\rm max,3,SF}$, bile flow, and SF dose are changed (C, D, H, I). Bile flow and SF dose are experimentally measured parameters that show an increase in biliary SF as their values are increased as expected, corroborating the model proposed in Fig. 3. $V_{\rm max,2}$, however, shows an increase in biliary SF upon decrease of this parameter. Finally, $V_{\rm max,3,SF}$ shows a large change in biliary SF that is directly proportional to the change in parameter. These results corroborate the findings presented in Fig. 4C and indicate which model parameters can be fixed for parsimony and model reduction (i.e., $V_{\text{max,1,SF}}$, β_1 , and β_2). SF, sodium fluorescein.



Given the large number of unknown model parameters relative to datapoints, we sought to reduce the model's complexity by fixing parameters whose variation led to little change in the simulated perfusate and bile SF time courses. It is clear from Fig. 5, A, B, and E, that changing $V_{\text{max.1.SF}}$, $V_{\text{max,1,SFG}}$, and $V_{\text{max,3,SFG}}$ elicited little variation in the simulated perfusate and bile SF time courses. This information is corroborated by the sensitivity plots in Fig. 4C. Based on this analysis, together with the analysis in Fig. 4, A and C, these parameters were fixed to their course-grained estimated values in Table 2. Thus, a three-parameter reduced model was developed where only $V_{\text{max,2}}$, $V_{\text{max,3,SF}}$, and α were estimated. There is a slight sensitivity of the perfusate curve to changes in α (Fig. 5F), particularly around the early timepoints (t =0–20 min). As α is related to reservoir mixing, and thus an experimentally determined parameter, we expected this parameter to show some variability between experiments and, thus, allowed it to vary in the reduced model.

Fitting of Reduced Ex Vivo MP Model to Average **Control and IRI Datasets**

Next, given the excellent fit of the original six-parameter model to the datasets, we tested the ability of the reduced three-parameter model to fit the control and IRI datasets (Fig. 6). Fitting of the control dataset with the three-parameter model yielded nearly perfect fits, similar to the six-parameter model (SSE₆ = 0.00341, SSE₃ = 0.00346; F =0.0406, P = 0.99) supporting model reduction from six to three parameters for the sake of model parsimony. Next, the 10-min WIT (I10), 20-min WIT (I20), and 30-min WIT (I30) SF time courses were fitted using the reduced three-parameter model (Fig. 6). Fitting of the I10 and I20 SF time courses

yielded nearly perfect fits, similar to the fit of the control dataset. Although the model does run through all the error bars for the 30-min WIT (I30) SF time course, the fit is qualitatively not as good as the fits for the other SF time courses. There are many likely explanations for this phenomenon. First, the I30 SF time-course data have a much higher global variability than the other datasets, indicating that there may be factors that the model has not accounted for. A smaller bile flow rate and a subsequent smaller collected bile volume may have contributed to the variability in the I30 dataset. As can be seen in Supplemental Table S1, the bile flow rates for the I30 condition are, overall, smaller than those for the control, I10, and I20 conditions, indicating reduced bile formation and secretion and reduced biliary region volume. Our model assumes a constant 0.4% of hepatic volume as biliary duct volume. Thus, given the same collection time, this yields a smaller total volume for fluorescence measurement and potentially is a contributor to the variability present in the I30 dataset, which is not considered in the model.

Fitting of Ex Vivo MP Model to Individual Datasets and Analysis of Model Parameters

Finally, we wanted to assess our model's robustness with respect to experimental and biological variability. Thus, using individualized rat parameters (e.g., total rat and liver weights and bile flow rates), we fit the three-parameter model schematized in Fig. 3 to the individual concentration datasets in Supplemental Fig. S2 and obtained estimates for $V_{\rm max,2}$, $V_{\rm max,3,SF}$, and α for each biological replicate. The results of these 21 fittings are shown in Supplemental Fig. S3. For verification, each of the three estimated and rat physiological parameters were averaged over each biological

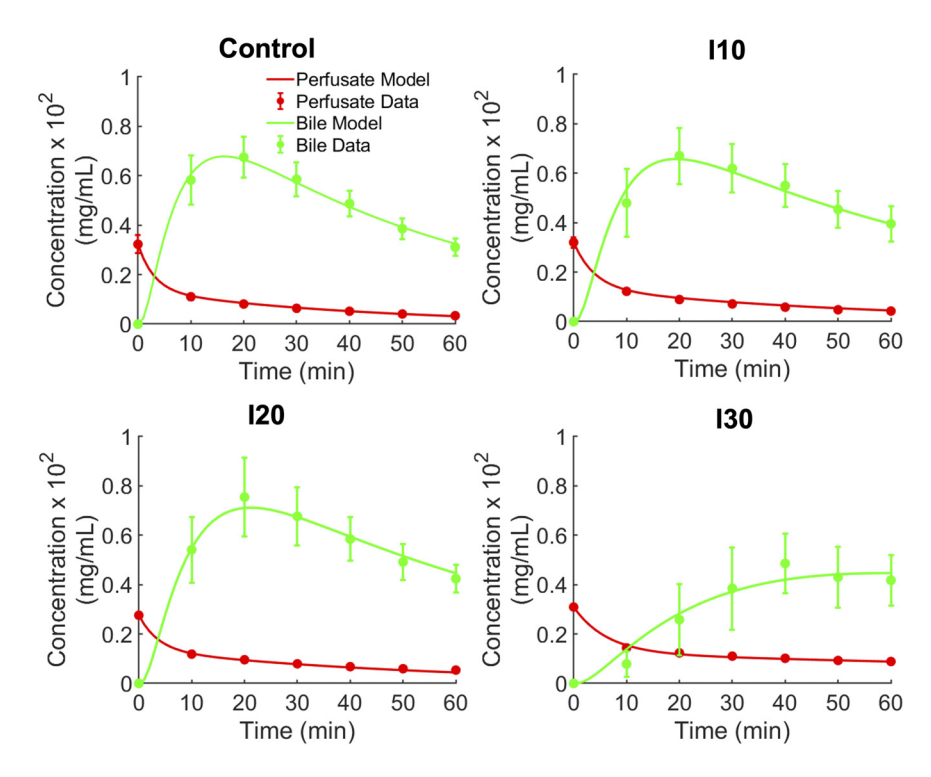


Figure 6. Fitting of the reduced three-parameter PBPK ODE model (see Figs. 4C and 5) to each dataset presented in Fig. 2B using pseudo-Monte Carlo parameter estimation approach (34). The estimated parameter values are presented in Table 3. ODE, ordinary differential equation; PBPK model, physiologically based pharmacokinetic model.

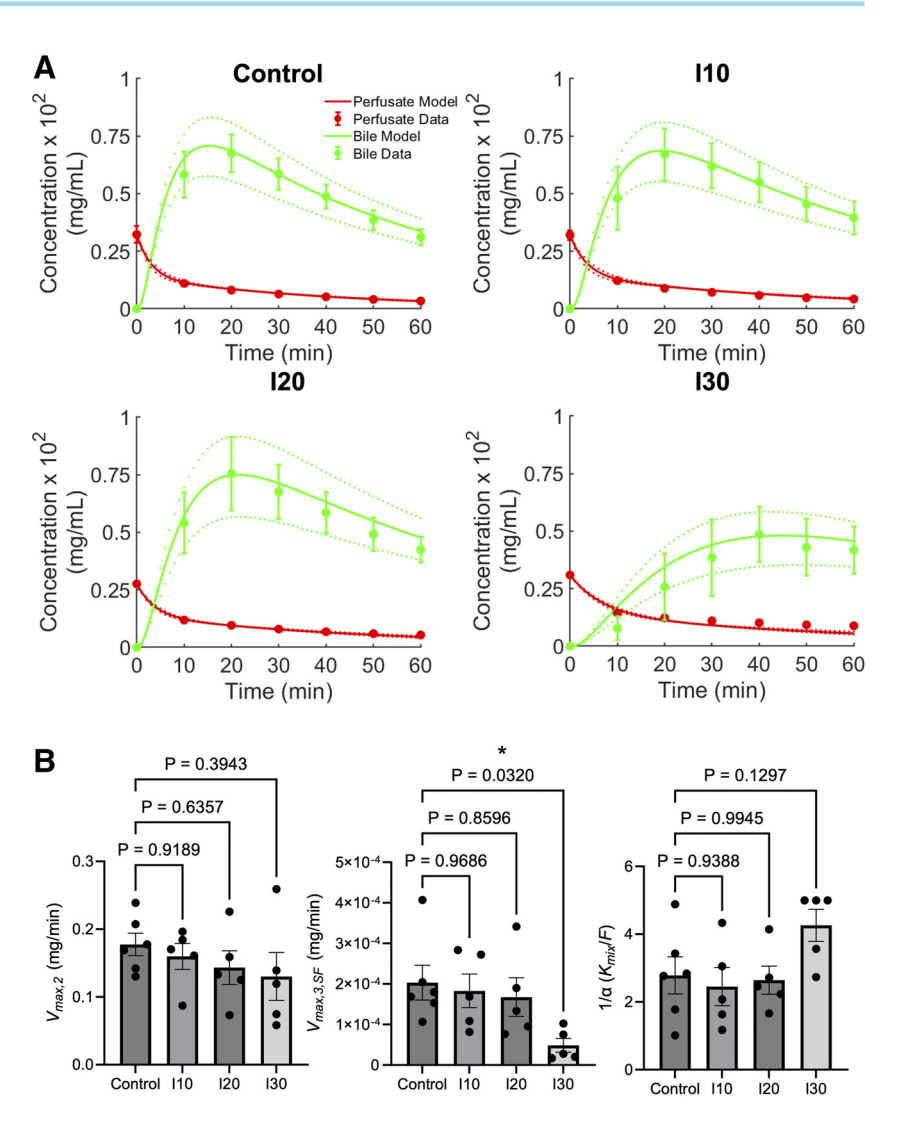
replicate, and the model was simulated using these average parameters and compared with mean data (Fig. 7A, solid curves). The standard error (SE) for each parameter was also calculated. The dotted curves in Fig. 7A represent model simulations using the parameters ± SE. Estimated model parameters are compared in Fig. 7B using a one-way ANOVA corrected for multiple comparisons using the Dunnett test. Comparisons of all estimated model parameters to control yielded nonsignificant results, except for $V_{\text{max,3,SF}}$, which was significantly smaller than the control value for the I30 condition. This result is in accordance with previously determined clinical findings, which suggest that a WIT of >20 min correlates with liver graft failure (12). We attempted to determine if the functional changes determined by modeling corresponded with changes observable through hematoxylin-eosin (H&E) staining and histologic evaluation. Paraffinembedded sections from each biological replicate were stained with H&E and examined by a trained pathologist (W.L.) using the Suzuki scoring algorithm (38). We were unable to find any histologic evidence of IRI as determined by Suzuki score (Supplemental Fig. S4 and Supplemental Table S2). These findings may suggest that changes in biliary function (i.e., a decrease in $V_{\text{max,3,SF}}$) may precede histologic evidence of IRI.

DISCUSSION

In this study, we 1) used an in-house experimental datadriven physiologically based pharmacokinetic (PBPK) computational modeling approach to generate a parsimonious PBPK model of ex vivo liver machine perfusion (MP) (Figs. 2-5), 2) fit this model to liver MP sodium fluorescein (SF) time-course datasets with varying amounts of warm ischemia time (WIT) (Figs. 6 and 7), and 3) compared estimates of critical model parameters by fitting the PBPK liver MP model to individual biological replicates using parameters obtained for each rat liver (Fig. 7 and Supplemental Fig. S3). We found that 1) ex vivo SF hepatic transport and biliary excretion kinetics can be described using a three-parameter version of the model proposed in Ref. 10 modified to account for MP livers (Figs. 3-5), 2) this model can also be appropriately adjusted via fitting to account for increasing WIT leading to increased hepatic ischemia-reperfusion injury (IRI) (Figs. 6 and 7), and 3) of the three critical parameters that were adjusted for fitting to the IRI SF datasets, only the maximal transport velocity of MRP2 for SF ($V_{\text{max,3,SF}}$) was sensitive to a WIT of >20 min (Fig. 7B).

The results of our modeling studies demonstrated qualitatively similar results to those shown in previous studies (39). There is some quantitative deviation between the results presented in this study and previous studies, which can likely be attributed to the fact that previous studies were conducted in situ as opposed to ex vivo (39). Overall, these results provide corroborative evidence that strengthens the relationship between decreased SF hepatic transport and biliary excretion with increasing WIT that has previously been established in the literature (10, 15). Furthermore, these studies examined the SF/WIT relationship in a different system and yielded similar results as previous work (10, 15). This evidence supports generalization of the SF/WIT relationship and the foundational "liver-centric" model proposed in Ref. 10. In that light, future modeling-based research may focus on scaling our ex vivo MP liver PBPK model to account for human liver physiology or applying the liver-centric model to different scenarios such as integration into a PBPK model accounting for whole body physiology. In addition, the livercentric model may be expanded to account for the spatial heterogeneity in liver ultrastructure as in Ref. 40 to help

Figure 7. Fitting of the three-parameter PBPK ODE model to each individual SF time-course datasets (see Supplemental Fig. S2). A: recapitulation of mean fitting using mean of individual parameters ± SE. The threeparameter PBPK ODE model was fit to the individual time-course datasets in Supplemental Fig. S2 (see Supplemental Fig. S3). Parameters for $V_{\rm max,3,SF}$, $V_{\rm max,3,SF}$, and α were estimated. Parameters were pooled for each condition and averaged, and the model was simulated using the mean parameter set (solid curves) and then compared with the mean data ± SE (see Fig. 2B). The model was then resimulated using the mean parameter set ± SE for each parameter (dotted curves). B: comparison of the estimated model parameter values for increasing values of WIT. $V_{\text{max.3.SF}}$ was the only parameter showing a statistically significant difference from control at the 30-min WIT (P value adjusted for multiple comparisons = 0.0320, which is less than the a priori determined α value of 0.05). ODE, ordinary differential equation; PBPK model, physiologically based pharmacokinetic model; SF, sodium fluorescein; WIT, warm ischemia time.



understand the susceptibility of hepatic zones to IRI. Future experimental and clinical studies may focus on detecting changes in SF hepatic transport and biliary excretion during ex vivo MP and using this information to back-calculate WIT using the PBPK model developed in this study. Ultimately, back-calculating WIT from SF excretion could be used to define an "effective warm ischemia time" (WITeff) that could subsequently be used as a clinical heuristic by surgeons to quantitatively assess donor organ viability. A WITeff for a donor liver that is below a well-defined threshold may help guide clinicians, in the correct clinical context, to use a donor liver that, under current guidelines, may otherwise be considered unsuitable for transplant. Functional WIT is currently determined using various hemodynamic and oxygenation parameters in the context of donation after circulatory death (11). An assessment of donor livers through effective WIT (WIT_{eff}) may enhance our understanding of the biological impact of functional WIT, providing a more precise evaluation of ischemic damage and organ viability. This approach suggests that integrating WIT_{eff} as a metric could bridge the gap between clinical observations and biological outcomes, potentially leading to improved strategies for organ evaluation and utilization (41). In addition,

the transplant surgeon will likely need to integrate the WIT_{eff} findings with additional measurements of liver function (e.g., lactate clearance, aminotransferase levels, and pH) to obtain a more holistic assessment of liver function. For example, our laboratory has investigated trends in aminotransferase levels and other cytokine markers during MP to help assess the overall functional and inflammatory statuses of the donor liver prior to transplantation (4). Although the ultimate goal of integrating WIT_{eff} into standard clinical practice likely requires many future experiments and clinical trials, the work in this study helps to establish a quantitative and mechanistic relationship between SF excretion and WIT during ex vivo MP.

Computational modeling is an important tool for the discovery of emergent properties of complex biological systems (34). Through the iterative process of computational modeling, we were able to uncover three important properties of the liver-centric model proposed in Ref. 10 that were not considered in that original work.

The first emergent property was the idea of competition between SF and SFG for OATP1B2/MRP3 and MRP2 transporters. Although the original liver-centric model proposed in Ref. 10 hypothesized that SF and SFG used the same transporters to enter hepatocytes and bile, this model also assumed that there was a large number of transporters relative to the concentrations of SF and SFG. Formulation of model equations using this assumption allows for simpler flux equations. Although application of this assumption to flux equations may effectively describe these experimental data, this assumption ignores the possibility of competition between the two molecules for a single transporter. This effect, which is well established, may come into play as the interaction between differing pathologies (i.e., steatosis and IRI) and their effects on transplant viability are investigated (25, 26, 39). Thus, to facilitate future modeling efforts and for a more holistic mathematical description of the transport kinetics, SF/SFG competition was integrated into the transport flux equations (*Egs. 5* and 6). Future studies could focus on the use of a competitive MRP2 inhibitor to mimic the action of SFG competition in combination with a potent inhibitor of hepatic glucuronidation to nullify the background effects of endogenously produced SFG to experimentally confirm this hypothesized mechanism.

The second emergent property about the ex vivo liver MP system presented in this study was the idea of incomplete mixing in the reservoir. During the model design phase, we had initially only incorporated one reservoir. Although this design gave a rough estimate of the data, key datapoints at time 0 and around the inflection point of the perfusate curve (t = 10-30 min) were systematically missed after fitting. To account for this, we hypothesized that once SF was injected into the top of reservoir 1, there was a small delay for it to be completely mixed into reservoir 2 and communicate with other components of the MP system. Although this may seem to be a minor, technical detail, it is important to consider incomplete mixing to avoid systematic error in future studies.

The third emergent property was the ratio of the maximal transport velocities ($V_{\rm max}$) associated with SFG and SF. For both $V_{\text{max},1}$ and $V_{\text{max},3}$, we found that the ratios of the V_{max} es for SFG to SF were estimated to be >1, indicating that SFG was transported more readily than SF. As mentioned previously, this may be due to the increased hydrophilicity of SFG relative to SF leading to faster transport across the hepatocyte membrane on both the sinusoid and canalicular sides of the cell (see RESULTS).

Although the studies presented in this article represent a thorough analysis of the data provided, there are still several limitations. First, Fig. 2B shows that as WIT increases, the overall variability in the SF measurements in the bile also increases. This is particularly apparent at the 30-min WIT. This may be due to the sluggish bile flow rates for that condition (see Table 3 and Supplemental Table S1), as it is likely more difficult to make measurements with such a small volume of bile. This could be remedied by the addition of variable volume for the biliary duct region or a higher concentration of choleretic agents in future experiments (4, 42). Moreover, this fact may be symptomatic of globally diminished bile production that is directly related to the hepatic IRI (14). In addition, as mentioned earlier, a WIT of >20 min has been associated with failure of liver transplantation in humans (12). It is reasonable to hypothesize that normal cell death processes such as breakdown of hepatocyte membranes occur after the withdrawal of critical nutrients

and oxygen and buildup of toxic metabolites that occurs during ischemia (43). Thus, the membranes that normally effectively compartmentalize SF into the sinusoids, hepatocytes, and bile may not be as effective as they are in the control, I10, and I20 conditions, allowing for SF to more freely equilibrate between model regions. As OATP1B2/MRP3 and MRP2 are membrane transporters, damage to the membrane could easily be extended to damage to the transporters themselves (44, 45). Moreover, mitochondrial damage is also cited to be a factor in hepatic ischemic injury (43). A paucity of energetic compounds such as ATP could lead to a decrease in MRP2 transport velocity (since MRP is an ATP-dependent pump), leading to the blunted response as seen in the lower right panel of Fig. 6. Future in vitro research is likely required to definitively determine the precise mechanism of hepatic ischemic injury. It is clear from Fig. 6, however, that SF biliary kinetics differ in the I30 condition compared with the control, I10, and I20 conditions.

Second, although the smaller production of bile may be unavoidable, optimization of the experimental procedure may involve optimizing SF doses to facilitate measurement by ensuring the concentrations being tested are within the linear range of the fluorescence assay or changing the detection method altogether to a chromatographic or mass spectrometry-based assay. Although these detection methods may increase sensitivity and are acceptable for laboratory-based research, they are generally more costly, and further optimization will be necessary for implementation in the clinic if more complex detection methods are applied. Third, in this study, all data relating to SFG were predictions based on the output of our ex vivo MP PBPK model. Future studies could focus on obtaining time courses for both SF and SFG to further refine the model proposed in these studies.

Fourth, the MP system used in this study was custom built by experimentalists to facilitate computational modeling studies. Other laboratories attempting to replicate and expand upon our studies may find it necessary or prudent to optimize the MP system for their conditions. In doing so, model parameters such as α are likely to change significantly. Furthermore, it may be necessary to use partial differential equations to more accurately describe the data obtained from a modified MP system if large amounts of tubing are used (23). Finally, throughout this discussion, we briefly discussed potential clinical applications of this study's findings. Although immediate application is limited and rigorous testing is necessary for clinical adoption, the foundational information presented herein paves the way for further research and subsequent clinical trials.

In conclusion, we developed a PBPK model of SF excretion kinetics from perfusate into bile in ex vivo MP rat livers subjected to varying amounts of IRI. Through these studies, we were able to identify that the transport velocity of the hepatic transporter MRP2 was significantly reduced from baseline at 30 min of WIT. Using PBPK modeling allowed for a nuanced interpretation of changes in SF kinetics due to modified MRP2 activity during IRI, an insight not immediately evident from raw experimental data. This refinement enhances our ability to interpret complex biological transport systems, paving the way for more accurate experimental analyses.



DATA AVAILABILITY

The model is developed in MATLAB. The MATLAB code and the associated data files used to generate all the results in this study as well as the Supplemental Materials can be found at https://github.com/MCWComputationalBiologyLab/Monti_ExVivo_ MP 2024. The MATLAB code and the datasets analyzed during the current study can also be obtained from the corresponding authors on request.

SUPPLEMENTAL MATERIAL

Supplemental Figs. S1-S4 and Tables S1 and S2: https:// figshare.com/s/480f8e49bbbcf6721ae0.

ACKNOWLEDGMENTS

The authors thank the reviewers for helpful comments to improve the quality of this article. BioRender was used to generate the Graphical Abstract.

GRANTS

This work was supported by National Institutes of Health Grant F30Al179084 (to C.E.M.) and National Science Foundation Grant DMS 2153387 (to R.K.D.).

DISCLOSURES

No conflicts of interest, financial or otherwise, are declared by the authors.

AUTHOR CONTRIBUTIONS

C.E.M., S.S.T., J.K., and R.K.D. conceived and designed research; S.-K.H., S.S.T., and J.K. performed experiments; C.E.M., S.-K.H., W.L., S.S.T., J.K., and R.K.D. analyzed data; C.E.M., S.-K.H., S.H.A., W.L., S.S.T., J.K., and R.K.D. interpreted results of experiments; C.E.M., S.H.A., W.L., J.K., and R.K.D. prepared figures; C.E.M., J.K., and R.K.D. drafted manuscript; C.E.M., S.-K.H., S.H.A., W.L., A.J., S.S.T., J.K., and R.K.D. edited and revised manuscript; C.E.M., S.-K.H., S.H.A., W.L., A.J., S.S.T., J.K., and R.K.D. approved final version of manuscript.

REFERENCES

- Zarrinpar A, Busuttil RW. Liver transplantation: past, present and future. Nat Rev Gastroenterol Hepatol 10: 434-440, 2013. doi:10. 1038/nrgastro.2013.88.
- 2. Saeian K, Shaker R. Liver Disorders: A Point of Care Clinical Guide. New York, NY: Springer, 2017
- Selck FW, Deb P, Grossman EB. Deceased organ donor characteristics and clinical interventions associated with organ yield. Am J Transplant 8: 965–974, 2008. doi:10.1111/j.1600-6143.2008.02205.x.
- Kim J, Hong S-K, Yang Y, Lee A, Hoffmeister KM, Gantner BN, Park J-I. Prolonged warm ischemia time increases mitogen-activated protein kinase activity and decreases perfusate cytokine levels in ex vivo rat liver machine perfusion. Front Transplant 2: 1215182, 2023. doi:10.3389/frtra.2023.1215182.
- Ojo AO, Heinrichs D, Emond JC, McGowan JJ, Guidinger MK, Delmonico FL, Metzger RA. Organ donation and utilization in the USA. Am J Transplant 4, Suppl 9: 27-37, 2004. doi:10.1111/j.1600-
- Gentry SE, Chow EK, Massie A, Luo X, Zaun D, Snyder JJ, Israni AK, Kasiske B, Segev DL. Liver sharing and organ procurement organization performance. Liver Transpl 21: 293-299, 2015. doi:10.1002/lt.24074.
- Ploeg RJ, D'Alessandro AM, Knechtle SJ, Stegall MD, Pirsch JD, Hoffmann RM, Sasaki T, Sollinger HW, Belzer FO, Kalayoglu M.

- Risk factors for primary dysfunction after liver transplantation-a multivariate analysis. Transplantation 55: 807-813, 1993. doi:10.1097/ 00007890-199304000-00024.
- Lentsch AB, Kato A, Yoshidome H, McMasters KM, Edwards MJ. Inflammatory mechanisms and therapeutic strategies for warm hepatic ischemia/reperfusion injury. Hepatology 32: 169-173, 2000. doi:10.1053/jhep.2000.9323.
- Zhai Y, Petrowsky H, Hong JC, Busuttil RW, Kupiec-Weglinski JW. Ischaemia-reperfusion injury in liver transplantation-from bench to bedside. Nat Rev Gastroenterol Hepatol 10: 79-89, 2013. doi:10. 1038/nrgastro.2012.225.
- Monti C, Audi SH, Womack J, Hong SK, Yang Y, Kim J, Dash RK. Physiologically-based pharmacokinetic modeling of blood clearance of liver fluorescent markers for the assessment of the degree of hepatic ischemia-reperfusion injury. Annu Int Conf IEEE Eng Med Biol Soc 2023: 1-6, 2023. doi:10.1109/EMBC40787.2023.10340273.
- Kalisvaart M, Schlegel A, Umbro I, de Haan JE, Scalera I, Polak WG, IJzermans JNM, Mirza DF, Perera M, Isaac JI, Ferguson J, Mitterhofer AP, de Jonge J, Muiesan P. The impact of combined warm ischemia time on development of acute kidney injury in donation after circulatory death liver transplantation: stay within the golden hour. Transplantation 102: 783-793, 2018. doi:10. 1097/TP.0000000000002085.
- Hong JC, Yersiz H, Kositamongkol P, Xia VW, Kaldas FM, Petrowsky H, Farmer DG, Lipshutz G, Markovic D, Hiatt JR, Busuttil RW. Liver transplantation using organ donation after cardiac death: a clinical predictive index for graft failure-free survival. Arch Surg 146: 1017-1023, 2011. doi:10.1001/archsurg.2011.240.
- Gaurav R, Butler AJ, Kosmoliaptsis V, Mumford L, Fear C, Swift L, Fedotovs A, Upponi S, Khwaja S, Richards J, Allison M, Watson CJE. Liver transplantation outcomes from controlled circulatory death donors: SCS vs in situ NRP vs ex situ NMP. Ann Surg 275: 1156-1164, 2022. doi:10.1097/SLA.000000000005428.
- Brüggenwirth IMA, Porte RJ, Martins PN. Bile composition as a diagnostic and prognostic tool in liver transplantation. Liver Transpl 26: 1177-1187, 2020. doi:10.1002/lt.25771.
- Kim J, Yang Y, Hong SK, Zielonka J, Dash RK, Audi SH, Kumar SN, Joshi A, Zimmerman MA, Hong JC. Fluorescein clearance kinetics in blood and bile indicates hepatic ischemia-reperfusion injury in rats. Am J Physiol Gastrointest Liver Physiol 323: G126-G133, 2022. doi:10.1152/ajpgi.00038.2022.
- Grotte D, Mattox V, Brubaker R. Fluorescent, physiological and pharmacokinetic properties of fluorescein glucuronide. Exp Eye Res 40: 23-33, 1985. doi:10.1016/0014-4835(85)90105-8.
- Thorling C, Liu X, Burczynski F, Fletcher L, Roberts M, Sanchez W. Intravital multiphoton microscopy can model uptake and excretion of fluorescein in hepatic ischemia-reperfusion injury. J Biomed Opt 18: 101306, 2013. doi:10.1117/1.JBO.18.10.101306.
- De Bruyn T, Fattah S, Stieger B, Augustijns P, Annaert P. Sodium fluorescein is a probe substrate for hepatic drug transport mediated by OATP1B1 and OATP1B3. J Pharm Sci 100: 5018-5030, 2011. doi:10.1002/jps.22694.
- Dietrich K. The roles of MRP2, MRP3, OATP1B1, and OATP1B3 in conjugated hyperbilirubinemia. Drug Metab Dispos 42: 561, 2014. doi:10.1124/dmd.113.055772.
- Scheffer GL, Kool M, de Haas M, de Vree JML, Pijnenborg ACLM, Bosman DK, Oude Elferink RPJ, van der Valk P, Borst P, Scheper RJ. Tissue distribution and induction of human multidrug resistant protein 3. Lab Invest 82: 193-201, 2002. doi:10.1038/ labinvest.3780411.
- Zamek-Gliszczynski MJ, Xiong H, Patel NJ, Turncliff RZ, Pollack GM, Brouwer KLR. Pharmacokinetics of 5 (and 6)-carboxy-2',7'-dichlorofluorescein and its diacetate promoiety in the hliver. J Pharmacol Exp Ther 304: 801-809, 2003. doi:10.1124/ ipet.102.044107.
- Ban D, Kudo A, Sui S, Tanaka S, Nakamura N, Ito K, Suematsu M, Arii S. Decreased Mrp2-dependent bile flow in the post-warm ischemic rat liver. J Surg Res 153: 310-316, 2009. doi:10.1016/j. jss.2008.02.064.
- Audi SH, Linehan JH, Krenz GS, Dawson CA. Accounting for the heterogeneity of capillary transit times in modeling multiple indicator dilution data. Ann Biomed Eng 26: 914-930, 1998. doi:10.1114/1.138.
- Briggs GE, Haldane JB. A note on the kinetics of enzyme action. Biochem J 19: 338-339, 1925. doi:10.1042/bj0190338.

- 25. Sadri S, Tomar N, Cowley AW Jr, Audi SH, Dash RK. Integrated computational modeling of the kinetics and regulation of NADPH oxidase 2 assembly, activation, electron flow, and superoxide production. FASEB J 34: 1-1, 2020. doi:10.1096/fasebj.2020.34.s1.02644.
- Pradhan RK, Vinnakota KC, Beard DA, Dash RK. Carrier-mediated transport through biomembranes. In: Transport in Biological Media, edited by Becker SM, Kuznetsov AV. Boston, MA: Elsevier, 2013, p. 181-212.
- Yang G, Ge S, Singh R, Basu S, Shatzer K, Zen M, Liu J, Tu Y, Zhang C, Wei J, Shi J, Zhu L, Liu Z, Wang Y, Gao S, Hu M. Glucuronidation: driving factors and their impact on glucuronide disposition. Drug Metab Rev 49: 105-138, 2017. doi:10.1080/ 03602532.2017.1293682.
- Dennis AS, Malcolm R. Intracellular and intraorgan concentrations of small molecule drugs: theory, uncertainties in infectious diseases and oncology, and promise. Drug Metab Dispos 47: 665, 2019. doi:10.1124/dmd.118.085951.
- Järvinen E, Deng F, Kiander W, Sinokki A, Kidron H, Sjöstedt N. The role of uptake and efflux transporters in the disposition of glucuronide and sulfate conjugates. Front Pharmacol 12: 802539, 2021. doi:10.3389/fphar.2021.802539.
- Nelson DL. Lehninger Principles of Biochemistry (4th ed.). New York: W.H. Freeman, 2005, p. 187-240.
- Hall C, Lueshen E, Mošat A, Linninger AA. Interspecies scaling in pharmacokinetics: a novel whole-body physiologically based modeling framework to discover drug biodistribution mechanisms in vivo. J Pharm Sci 101: 1221-1241, 2012. doi:10.1002/jps.22811.
- Luo Y, Mulder GB, Luo Y, Fisher TF. Validation of a Bile Duct Cannulation Rat Model. Wilmington, MA: Charles River, 2009
- Masyuk TV, Ritman EL, LaRusso NF. Quantitative assessment of the rat intrahepatic biliary system by 3-dimensional reconstruction. Am J Pathol 158: 2079-2088, 2001. doi:10.1016/S0002-9440(10) 64679-2.
- Monti CE, Mokry RL, Schumacher ML, Dash RK, Terhune SS. Computational modeling of protracted HCMV replication using genome substrates and protein temporal profiles. Proc Natl Acad Sci USA 119: e2201787119, 2022. doi:10.1073/pnas.2201787119.
- Byrd RH, Gilbert JC, Nocedal J. A trust region method based on interior point techniques for nonlinear programming. Math Program 89: 149-185, 2000. doi:10.1007/PL00011391.
- Motulsky H, Christopoulos A. Fitting Models to Biological Data using Linear and Nonlinear Regression: A Practical Guide to Curve Fitting. New York, NY: Oxford University Press, 2003.

- Riveros S, Marino C, Ochoa G, Morales E, Soto D, Alegría L, Zenteno MJ, Brañes A, Achurra P, Rebolledo RA. Implementation and design of customized ex vivo machine perfusion. Analysis of its first results. Artif Organs 46: 210-218, 2022, doi:10.1111/aor.14060.
- Sosa RA, Zarrinpar A, Rossetti M, Lassman CR, Naini BV, Datta N, Rao P, Harre N, Zheng Y, Spreafico R, Hoffmann A, Busuttil RW, Gjertson DW, Zhai Y, Kupiec-Weglinski JW, Reed EF. Early cytokine signatures of ischemia/reperfusion injury in human orthotopic liver transplantation. JCI Insight 1: e89679, 2016. doi:10.1172/ jci.insight.89679.
- Thorling CA, Jin L, Weiss M, Crawford D, Liu X, Burczynski FJ, Liu D. Wang H. Roberts MS. Assessing steatotic liver function after ischemia-reperfusion injury by in vivo multiphoton imaging of fluorescein disposition. Drug Metab Dispos 43: 154-162, 2015. doi:10.1124/
- Franiatte S, Clarke R, Ho H. A computational model for hepatotoxicity by coupling drug transport and acetaminophen metabolism equations. Int J Numer Method Biomed Eng 35: e3234, 2019. doi:10.1002/
- Coffey JC. Wanis KN. Monbaliu D. Gilbo N. Selzner M. Vachharajani N, Levstik MA, Marquez M, Doyle MBM, Pirenne J, Grant D, Heimbach JK, Chapman W, Vogt K, Hernandez-Alejandro R. The influence of functional warm ischemia time on DCD liver transplant recipients' outcomes. Clin Transplant 31: e13068, 2017. doi:10.1111/ctr.13068.
- Lee TH, Han JH, Kim HJ, Park SM, Park SH, Kim SJ. Is the addition of choleretic agents in multiple double-pigtail biliary stents effective for difficult common bile duct stones in elderly patients? A prospective, multicenter study. Gastrointest Endosc 74: 96-102, 2011. doi:10. 1016/j.gie.2011.03.005.
- Konishi T, Lentsch AB. Hepatic ischemia/reperfusion: mechanisms of tissue injury, repair, and regeneration. Gene Expr 17: 277-287, 2017. doi:10.3727/105221617X15042750874156.
- Fang Z, Huang J, Chen J, Xu S, Xiang Z, Hong M. Transmembrane domain 1 of human organic anion transporting polypeptide 2B1 is essential for transporter function and stability. Mol Pharmacol 94: 842-849, 2018. doi:10.1124/mol.118.111914.
- Jedlitschky G, Hoffmann U, Kroemer HK. Structure and function of the MRP2 (ABCC2) protein and its role in drug disposition. Expert Opin Drug Metab Toxicol 2: 351-366, 2006. doi:10.1517/ 17425255.2.3.351.